

Mock observations with the Millennium simulation: Cosmological downsizing and intermediate redshift observations

M. J. Stringer^{1,3}, A. J. Benson¹, K. Bundy², R. S. Ellis^{1,3}, E. L. Quetin¹

1. Caltech, 1200 E. California Blvd., Pasadena, CA 91125, U.S.A.

2. Dept. of Astronomy and Astrophysics, University of Toronto, 50 St. George Street, Rm 101, Toronto, ON, M5S 3H4, Canada

3. Department of Astrophysics, Keble Rd., Oxford, OX1 3RH, U.K.

31 October 2021

ABSTRACT

Only by incorporating various forms of feedback can theories of galaxy formation reproduce the present-day luminosity function of galaxies. It has also been argued that such feedback processes might explain the counter-intuitive behaviour of ‘downsizing’ witnessed since redshifts $z \simeq 1$ -2. To examine this question, observations spanning $0.4 < z < 1.4$ from the DEEP2/Palomar survey are compared with a suite of equivalent mock observations derived from the Millennium Simulation, populated with galaxies using the GALFORM code. Although the model successfully reproduces the observed total mass function and the general trend of ‘downsizing’, it fails to accurately reproduce the colour distribution and type-dependent mass functions at all redshifts probed. This failure is shared by other semi-analytical models which collectively appear to “over-quench” star formation in intermediate-mass systems. These mock lightcones are also a valuable tool for investigating the reliability of the observational results in terms of cosmic variance. Using variance estimates derived from the lightcones we confirm the significance of the decline since $z \sim 1$ in the observed number density of massive blue galaxies which, we argue, provides the bulk of the associated growth in the red sequence. We also assess the limitations arising from cosmic variance in terms of our ability to observe mass-dependent growth since $z \sim 1$.

1 INTRODUCTION

The physical picture of how galaxies assemble has changed markedly over the past decade. A pure ‘hierarchical dark matter model’ in which gas cooling and subsequent star formation occurs in synchronisation with the growth, via gravitational instability, of their parent dark matter halos fails to reproduce the local luminosity function of galaxies (Benson et al. 2003; Somerville & Primack 1999; Kauffman et al. 1999) and has been challenged by the presence of massive ($\simeq 10^{11} M_{\odot}$) galaxies at redshifts $z \simeq 2$ (Glazebrook et al. 2004; Cimatti et al. 2004; van Dokkum et al. 2006). As a result, a new paradigm has emerged which argues for the importance of ‘feedback’ processes that serve to govern the star formation rate in a galaxy. As the efficacy of these processes depends on the mass of the host galaxy, so it is possible to reconcile the predictions of the standard CDM model with the local galaxy luminosity function (Croton et al. 2006; Bower et al. 2006).

Despite this progress, the physical basis of the feedback processes incorporated into the recent semi-analytic models remains largely untested. The most effective way of suppressing star formation and hence inhibiting further growth

in massive galaxies is “radio mode” feedback (Croton et al. 2006; Bower et al. 2006), where additional gas cooling in halos in which the cooling time is longer than the dynamical time is prevented by low levels of accretion onto central supermassive black holes. Bower et al. (2006) have argued that such a process can lead naturally to a characteristic mass scale associated with the transition between cooling on a hydrostatic timescale and more rapid cooling. Although such a feedback mode can be arranged to match the break in the present day luminosity function, a key issue is whether it explains the trajectory of star formation in galaxies over the past 5-10 Gyr.

Similar progress has been made observationally in measuring the evolving stellar mass function of galaxies over $0 < z < 1.5$, where large and complete samples can be obtained (Fontana et al. 2004; Drory, Bender & Hopp 2004; Bundy et al. 2006; Borch et al. 2006; Pozzetti et al. 2007). The advent of large-format near-infrared detectors used in conjunction with deep, spectroscopic and multi-wavelength surveys has characterized the evolving stellar mass function (Fontana et al. 2004), illuminated the bimodal nature of local galaxies (Kauffman et al. 2003), demonstrated the presence of morphological evolution associated with assembly

since $z \sim 1$ (Brinchmann & Ellis 2000) and revealed how the quenching of star formation in massive galaxies produces the downsizing signature (Bundy et al. 2006).

The time is therefore ripe for a direct confrontation between recent simulations which incorporate “radio mode” feedback to fit the local luminosity function and the history of mass assembly over $0 < z < 1.5$ from the new generation of deep surveys. By using stellar mass estimates as a bridge between theory and observations we can gain significant insight not only into the success of the physical prescriptions employed by these models (Kitzbichler & White 2006), but also the utility of observations in answering the questions posed above.

A key issue in comparing theoretical predictions with observations is the reliability of the latter. Previous comparisons (Kitzbichler & White 2007; Bower et al. 2006; Cole et al. 2001) have been content to compare the *total* stellar mass function. However, the signature of downsizing in star formation is most readily tested by examining the mass function partitioned into star-forming and quiescent populations (Bundy et al. 2006). While their fractional contributions are relatively easily measured, the absolute numbers of these sub-populations are less certain because of the limitations of cosmic variance. This must be properly understood in any comparison, whether it be theory versus data or one dataset against another.

As an example of the uncertainties arising from cosmic variance, we note that while it is generally accepted in the community that the number of red-sequence galaxies grows with time, confusion remains over whether this growth arises at the expense of a decline in the blue population (Bundy et al. 2006), or is dominated by “dry” mergers occurring within the red sequence, leaving the population of blue galaxies mostly invariant (Faber et al. 2007). In observational samples broken by redshift bin and galaxy class, the impact of cosmic variance becomes a critical issue, sufficient perhaps to explain differences in empirical interpretations. In this paper we will use numerical simulations not only to test popular models of feedback against observations, but also to evaluate rigorously the limitations in the data arising from cosmic variance.

Our work follows logically from the earlier study of Kitzbichler & White (2007). Those authors considered the output of lightcones drawn from semi-analytical models incorporating radio mode feedback as applied to the Millenium Simulation (Springel, White & Jenkins 2005) and compared predictions with various observables over $0 < z < 5$. They concluded broad agreement except in the abundance of high- z galaxies with large stellar masses. In this paper, we will focus on how star formation is distributed within the evolving galaxy population.

We construct an ensemble of 20 *lightcones* (§3.3) drawn from the GALFORM semi-analytic model (Bower et al. 2006) as applied to the Millennium Simulation. These lightcones are designed to mimic the Palomar/DEEP2 survey observations presented in Bundy et al. (2006) which we argue in §2 below is currently the best dataset for addressing the questions of differential mass assembly and evolution of star forming and quiescent galaxies. These lightcones include the detailed survey geometry, optical and K -band magnitude limits, and photometric as well as stellar mass uncertainties described in Bundy et al. (2006). Critically, by studying the

variation across our 20 realizations, we are also able to determine reliable estimates of the effect of cosmic variance. As we will show, this is key to an accurate comparison between models and data.

A plan of the paper follows. In §2 we justify our choice of the DEEP2/ Palomar spectroscopic stellar mass catalog (Bundy et al. 2006) as the comparison dataset. In §3 we discuss the Millenium Simulation and the associated GALFORM galaxy formation model. We review the various feedback mechanisms and illustrate how they lead, in principle, to the concept of downsizing. We then describe how we construct suitable lightcones and implement the effect of mass errors in the context of the observational data. We compare the predicted colour distribution with the observations and discuss the uncertainties associated with various ways of selecting active and quiescent galaxies. In §4 we compare our mass functions with the observations of Bundy et al. (2006). We also discuss our findings with regard to how cosmic variance may limit such conclusions, not only in the context of the current survey (Bundy et al. 2006) but also in other extant and projected surveys.

2 OBSERVATIONAL DATA

In this section we review the key features of the dataset presented in Bundy et al. (2006) which will serve as the “survey template” for constructing the lightcones described in §3 and the detailed comparisons discussed in §4.

In order to derive reliable stellar mass functions, there are two highly desirable observational ingredients - extensive multi-band photometry extending to the near-infrared, and spectroscopic redshifts for the majority of the sample. Although no existing survey has *complete* spectroscopic coverage down to the faintest luminosities probed, we will focus in particular on comparisons of the downsizing signature, so good coverage at the high mass end is certainly advantageous.

Our choice to focus on the DEEP2/Palomar catalog is motivated by a number of key advantages of this dataset. Foremost, as it builds on the extensive well-sampled DEEP2 Galaxy Redshift Survey (Davis et al. 2003), it satisfies the two major criteria above. Furthermore, with respect to the important issue of cosmic variance, the survey covers the largest area among published surveys with K -band imaging— 1.5 deg^2 spread over 4 independent fields. The COMBO17 survey (Wolf et al. 2003) covers ~ 0.8 square degrees in 3 fields, but has no near-infrared photometry. Although it has no spectroscopic coverage, it does benefit from highly-calibrated and well-tested photometric redshift data. The VVDS (Le Fèvre et al. 2005) data set presented in Pozzetti et al. (2007) samples only a single field with an area of ~ 0.5 square degrees, and only ~ 0.2 square degrees has K -band imaging.

We refer the reader to Bundy et al. (2006) for further details and only summarize the key aspects of the DEEP2/Palomar data set here. Palomar K_S -band photometry was obtained in portions of all four fields targeted by the DEEP2 Galaxy Redshift Survey. The Extended Groth Strip (EGS) was the top-priority field and contains the deepest observations. In Bundy et al. (2006) three different redshift intervals were constructed, $0.4 < z < 0.7$, $0.75 < z < 1.0$, $1.0 <$

Table 1. A summary of the observational sample (Bundy et al 2006).

Field		Number of Galaxies				Area/deg ²
		$0.4 < z < 0.7$	$0.75 < z < 1$	$1 < z < 1.4$	Total	
EGS	1	947	1004	722	2673	0.42
DEEP2	2	-	209	31	240	0.05
	3	-	353	266	619	0.13
	4	-	644	409	1053	0.14
Totals		947	2210	1428	4585	0.74

$z < 1.4$ with K_S -band depths corresponding to $K_{AB} = 21.8, 22.0$ and 22.2 for the three ascending redshift ranges. The lowest redshift sample comes entirely from the EGS, since galaxies with $z < 0.7$ were excluded through colour selection in the other DEEP2 fields. In all cases, DEEP2 redshift targets were limited to $R < 24.1$. The field sizes are listed in Table 1.

Central to our later discussion will be the partitioning of this sample into star-forming and quiescent galaxies. This is key to understanding the rate at which feedback suppresses star formation and provides valuable information in addition to the integrated stellar mass function (Kitzbichler & White 2007). Bundy et al. (2006) considered both the rest-frame $U - B$ colour and the rest-frame equivalent width of the [O II] emission line (Guzman et al. 1997) as proxies for the star formation rate.

3 MODELLING

Our aim in this work is to construct multiple sets of model galaxies selected in a similar manner, and with stellar masses inferred using similar techniques, as for the observed galaxies. This will provide the fairest possible comparison between theory and data.

3.1 Mass assembly

The model galaxy samples are generated from the population of dark matter halos in the Millennium Simulation (Springel, White & Jenkins 2005). This simulation consists of approximately 10 billion dark matter particles each of mass $8.6 \times 10^8 h^{-1} M_\odot$ evolving in a cubic volume of side $500 h^{-1} \text{Mpc}$, assuming a ΛCDM cosmology¹.

Dark matter halo merger trees are found from this 4-volume using the methods described by Harker et al. (2006). The lowest mass halos contained in these trees, of which there are about 20 million, consist of 20 particles corresponding to a total mass of $5 \times 10^9 h^{-1} M_\odot$. Such halos could contain at most $9 \times 10^8 h^{-1} M_\odot$ of baryonic material which is well below the lower limit of the stellar mass functions to be considered in this work. Therefore we do not expect the resolution of the Millennium Simulation to affect our results.

The assembly of dark matter halos in ΛCDM is often described as ‘‘hierarchical’’. This is appropriate in that some galaxies from one generation will merge to create the next.

¹ Specifically, a flat universe with $\Omega_b = 0.045, \Omega_M = 0.25, H_0 = 73 \text{km s}^{-1} \text{Mpc}^{-1}$ and $\sigma_8 = 0.9$.

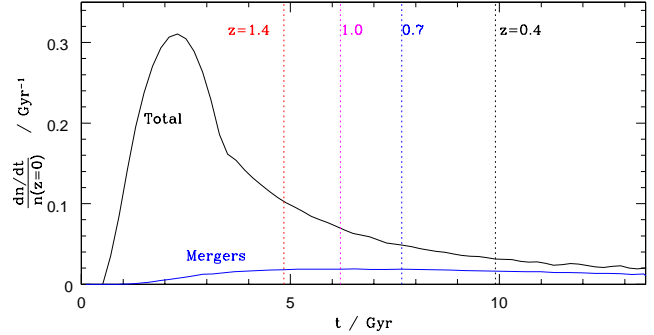


Figure 1. The formation rate of galaxies within the Millennium Simulation as a fraction of their present day number. The upper black line shows the total formation rate of galaxies with $M_\star > 10^9 M_\odot$, the lower blue line shows the rate at which pairs of these galaxies merge with each other. (Mergers involving smaller systems are not included.) The area between the curves will therefore be equal to one. Redshifts relevant to the DEEP2/Palomar samples are indicated with vertical dotted lines.

The importance of this contribution is illustrated in Figure 1. The detailed treatment of merging galaxies within a halo can be found in Bower et al. (2006).

The Millennium Simulation demonstrates that the merger rate is expected to be quite small; less than 2% of galaxies with $M_\star > 10^9 M_\odot$ merge with each other every Gyr. At early times, minor mergers and the formation of new stars therefore create massive galaxies much faster than they are destroyed by mergers and the latter effect is almost negligible. As the universe evolves, the creation rate of new galaxies diminishes, leading to a near zero net growth in numbers (the difference between the two curves in Figure 1). The growth trend is no longer in the number of galaxies but in their individual *stellar masses*.

When one considers the *differential* mass assembly, therefore, mergers become particularly important. Figure 2 shows the total number of galaxies formed up to a given redshift through accretion (equivalent to the ‘total’ component in Figure 1) alongside the number which remain after all mergers (since $t=0$) have taken place. The latter is the true, final number.

The number density of galaxies in a given mass range will rise or fall depending on whether more galaxies arrive or leave that range due to an increase in their stellar masses. At intermediate masses, the population is almost unaffected by mergers; the creation and destruction rates are approximately equal. At high mass, merging has a more significant effect because of the high ratio of potential progenitors to ex-

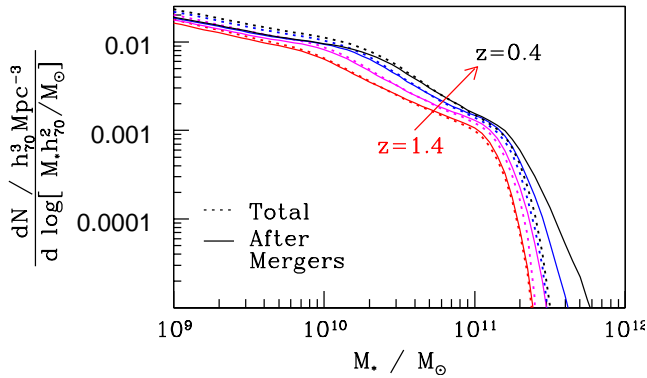


Figure 2. The evolving comoving number density of galaxies seen in the Millenium Simulation. Lines are coloured from black to red (top to bottom) corresponding to redshift limits ($z=0.4$, 0.7, 1.0 and 1.4) adopted in the DEEP2/Palomar survey. The total number of systems formed by a given redshift is shown as a dotted line whereas the associated solid line shows the true number, including mergers.

isting galaxies (indicated by a more steeply declining mass function at these masses). A particular deduction is that very massive galaxies ($M_* > 3 \times 10^{11} M_\odot$) would be almost non-existent without merging.

The preceding discussion is primarily based upon the formation and interaction of dark matter halos in the simulation. However, in order to construct Figure 2 we did have to consider the stellar content of the galaxies as well as their host halos. We now turn to discuss how stellar populations are introduced.

3.2 Galaxies

Halos in the merger trees introduced earlier are populated with galaxies using the GALFORM semi-analytic model, originally described by Cole et al. (2000). Here we use the implementation of that model described in detail by Bower et al. (2006). The reader is referred to Cole et al. (2000) and Bower et al. (2006) for a full description. Here we briefly summarise the key physical processes included.

The baryonic component of each dark matter halo is assumed to shock-heat during collapse of the halo to the virial temperature, at which point it settles into hydrostatic equilibrium and remains pressure supported until it can cool. The radius which has cooled at a given time after halo formation is calculated based on the metallicity of the gas, the cooling curve of Sutherland & Dopita (1993) and by assuming that it is isothermal at the virial temperature, with the radial density distribution:

$$\rho_{\text{gas}}(r) \propto (r^2 + r_{\text{core}}^2)^{-1}, \quad (1)$$

with r_{core} set equal to one tenth of the virial radius. This choice is motivated by the simulations of Eke et al. (1998) and Navarro, Frenk, & White (1995). If the free-fall time for this radius has already been passed, any remaining enclosed halo gas is assumed to have settled into the central disk, where it becomes rotationally supported by its residual angular momentum and the combined gravitational potential of the baryonic and dark matter. (The gas is otherwise added to the disk after a free-fall time).

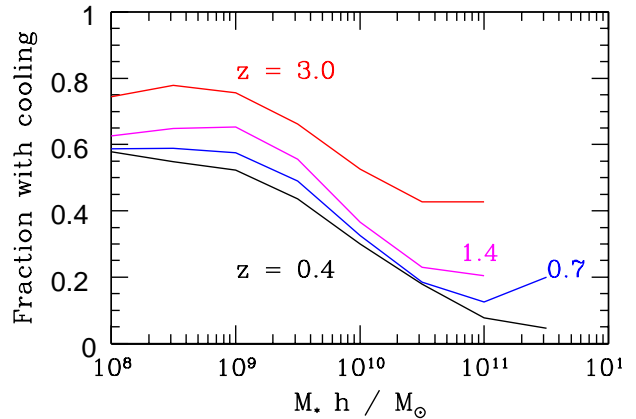


Figure 3. The fraction of galaxies with non-zero mass accretion due to cooling, plotted as a function of stellar mass, for four redshifts. The bottom three span the range of the DEEP2/Palomar samples. Significant cooling with subsequent star formation occurs for all masses at high redshift, declining to be almost completely suppressed for $M_* > 10^{11} M_\odot$ by $z \simeq 0.4$. This demonstrates how the continued suppression of star formation due to radio mode AGN feedback can reconcile downsizing in the context of hierarchical models.

We note that recent simulations have shown that, in low mass halos, shock heating may never occur, with gas arriving into the central galaxy through “cold flows” (Kereš et al. 2005; Birnboim & Dekel 2003). This mode of accretion is correctly accounted for in the model: In such low mass halos the cooling time will become much shorter than the halo dynamical time, and the mass infall rate will become independent of the assumption of shock heating and subsequent cooling and will instead be controlled by the cosmological mass accretion rate of the halo and the time required for free-fall.

Star formation then proceeds in this cold disk gas with an instantaneous rate, ψ given by:

$$\psi = \epsilon_* \left(\frac{v_{\text{disk}}}{200 \text{ km s}^{-1}} \right)^{\frac{3}{2}} \frac{M_{\text{gas}}}{\tau_{\text{disk}}}, \quad (2)$$

where τ_{disk} refers to the dynamical time in the disk, v_{disk} the circular velocity at the half-mass radius and the dimensionless efficiency parameter, $\epsilon_* = 0.0029$.

The key necessity for feedback arises because the above assumptions lead to overly rapid cooling and star formation and hence to a galaxy mass distribution incompatible with observations (Benson et al. 2003). Various physical mechanisms have been proposed to provide the necessary feedback effects to prevent this from occurring. Two processes are particularly important:

- **Reheating** of disk gas preferentially suppresses the formation of low-mass galaxies because of their shallow potential wells. Some fraction of the disk gas is reheated by stellar winds and supernovae and is instantaneously (relative to the other timescales within the model) returned to the halo. This process is parameterised as follows:

$$\dot{M}_{\text{out}} = \beta \psi, \quad \beta = \left(\frac{v_{\text{hot}}}{v_{\text{disk}}} \right)^{3.2} \quad (3)$$

with $v_{\text{hot}} = 485 \text{ km/s}$. β can become extremely large, exceeding 10^4 for small systems and approaching unity only for the most massive galaxies². This effect cannot, therefore, be ignored when discussing the efficiency of star formation. In fact, the process of reheating as described by eqn. (3) is ultimately responsible for determining the eventual star formation rate and not, as might be initially expected, the star formation process as described by eqn. (2). This is discussed further in Appendix A.

• **AGN heating** was introduced by Bower et al. (2006) and occurs if the halo free fall time is shorter than the cooling time (formally, $t_{\text{cool}} > \alpha_{\text{cool}} t_{\text{ff}}$, where $\alpha_{\text{cool}} = 0.58$ is an adjustable parameter) such that a hydrostatic halo can exist. If this condition is met, further cooling of gas is prevented if the Eddington luminosity of the super massive black hole residing at the centre of the galaxy greatly exceeds the cooling luminosity ($L_{\text{Edd}} > \epsilon_{\text{SMBH}}^{-1} L_{\text{cool}}$, where $\epsilon_{\text{SMBH}} = 0.04$ is an adjustable parameter). This strongly suppresses the formation of the most massive galaxies and imprints a near exponential cut-off in the abundance of the brightest galaxies. The two free parameters, α_{cool} and ϵ_{SMBH} , were chosen by Bower et al. (2006) by constraining the model to match local luminosity function data.

The black hole itself grows through gas accretion triggered by mergers and disk instabilities, acquiring $F_{\text{BH}} = 0.5\%$ of the available gas in each merger event and, similarly, 0.5% of the available gas in the galaxy if the disk’s self-gravity exceeds the critical limit,

$$\frac{GM_{\text{disk}}}{r_{\text{disk}}} > 0.8V_{\text{max}}, \quad (6)$$

thereby causing the disk to become unstable. This criterion follows the work of Efsthathiou, Lake & Negroponte (1982) though the particular constant, and the value of F_{BH} , was found by requiring the model to match the Magorrian relation between bulge mass and black hole mass, $M_{\text{BH}} \sim M_{\text{bulge}}^{1.12}$, as observed by Häring & Rix (2004).

AGN heating is expected to primarily suppress the formation of the most massive galaxies. As a consequence of hierarchical growth, such systems will have considerable spheroidal components and, hence, massive central black holes. A study of AGN feedback implemented in semi-analytic models has been made by Croton et al. (2006), also using the Millennium Simulation, who found qualitatively similar results.

² These values for β are extraordinary when viewed in the context of the physics thought to be involved in this outflow process. If eqn. (3) is taken to be energy conserving, so that the gravitational potential energy gained by the expelled gas comes directly from the stellar winds and supernovae, the energy acquired by the gas per star formed would be

$$E = \beta^{3/8} m_{\star} (485 \text{ km s}^{-1})^2. \quad (4)$$

For a typical IMF approximately one supernova is expected for every $100M_{\odot}$ of stars formed. This implies supernovae energies of about

$$E \approx \left(\frac{200 \text{ km/s}}{v_{\text{disk}}} \right)^{1.2} 10^{44} \text{ J}. \quad (5)$$

This will exceed the available supply for galaxies smaller than the Milky Way, even without considering the efficiency with which this is conveyed to the gas (McKee & Ostriker 1977).

Figure 3 illustrates the effect of AGN feedback³ in a simple way by showing the fraction of galaxies in the model with active cooling (i.e. those whose cooling has *not* been shut down by AGN heating). Cooling is largely unaffected in low-mass systems but is completely suppressed in the majority of massive systems. This illustrates how hierarchical structure formation can be made consistent with the observational phenomenon of ‘downsizing’.

In summary, in order for a galaxy to form a significant number of stars, there must be a supply of cooling gas from the surrounding halo to counteract the reheating of gas by the energy released. In this case equilibrium will quickly be reached which, under our particular parameterisation of the processes involved, results in a roughly constant specific star formation rate⁴ across all masses (see Fig. A1). However, this balance is only possible in that fraction of galaxies for which the energy from the AGN is insufficient to prevent cooling of halo gas. In the case of no cooling, the fuel for star formation will quickly be exhausted, causing the galaxy to fade and redden.

Thus, we can expect the galaxy population to be divided into two populations: those where cooling is occurring (high star formation rate, blue colours) and those with no cooling (little or no star formation, red colours). The relative abundance of each of these categories depends on the galaxies’ mass. The key question we wish to address is whether the growth and abundance of these two populations, which depends crucially on the feedback mechanism, matches that observed.

3.3 Lightcones

We use the prescriptions for gas cooling, star formation, and feedback described above to populate dark matter halos from the Millennium Simulation with model galaxies. The extremely large volume of this simulation allows us to reduce the statistical uncertainty in our predictions. However, to assess the significance of potential differences with observations we must examine various sources of uncertainty. While errors based on photometry or Poisson statistics are typically straightforward to estimate, the observational results of interest here—in particular, galaxy number density—are often dominated by sample or “cosmic” variance, which is much more challenging to quantify. The combination of a semi-analytic model and the Millennium Simulation provides a powerful approach to this problem. After demonstrating general agreement between simulated and observed results, we construct numerous mock datasets with the identical field geometry, magnitude limits, and photometric uncertainties as the real datasets. By comparing multiple realizations, we can accurately estimate the effect of cosmic variance. Below, we describe our method for constructing such lightcone datasets⁵.

³ Figure 7 of Croton et al. (2006) illustrates a related point by showing the effect of AGN feedback in their model on the mean behaviour of all galaxies rather than the fraction which is affected.

⁴ Specific star formation rate $\equiv \dot{M}_{\star}/M_{\star}$.

⁵ Such datasets are referred to as “lightcones” (Kitzbichler & White 2007) as they contain all galaxies which intersect the past

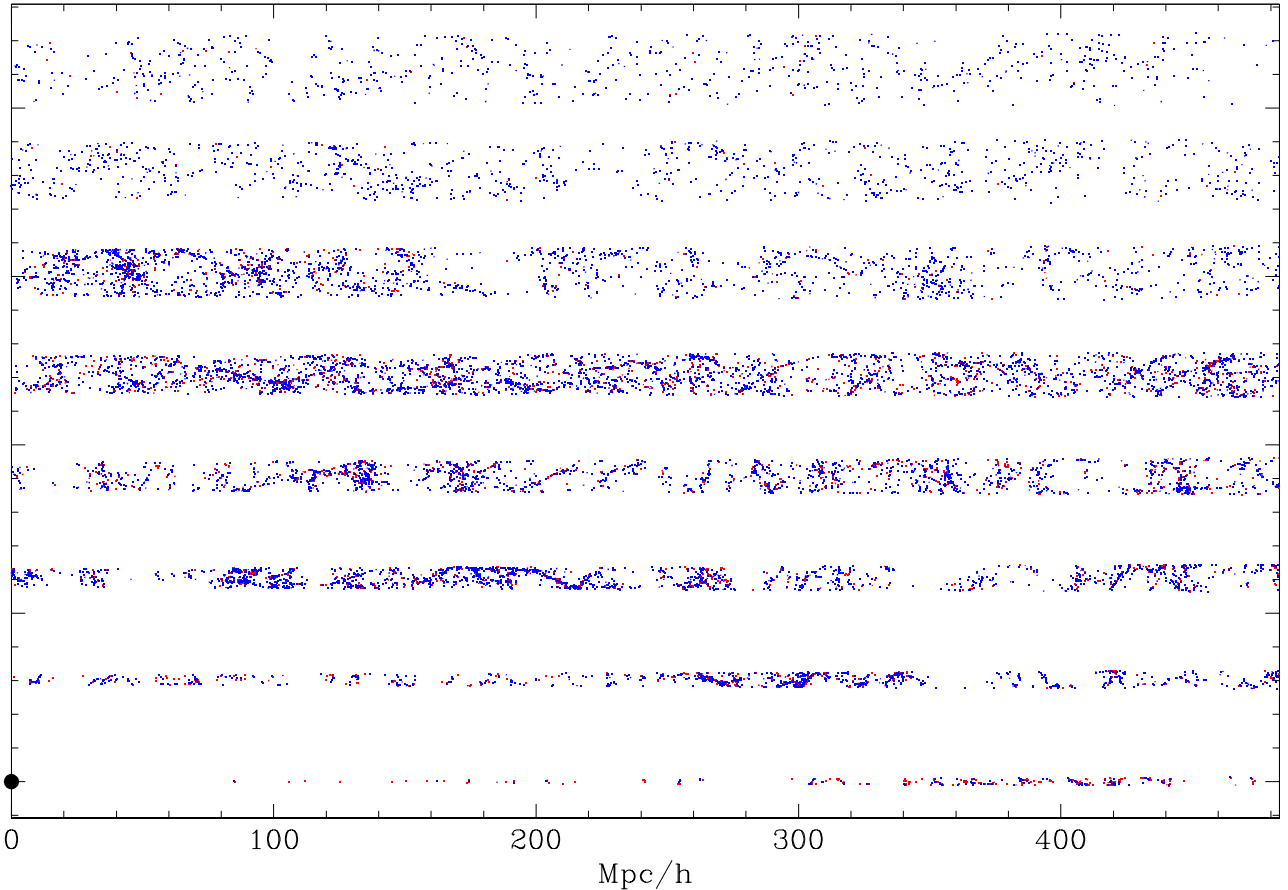


Figure 4. Projection of a sample of galaxies on a lightcone drawn from the $\sim 10^8 \text{Mpc}^3$ comoving volume of the Millennium Simulation. To mimic the DEEP2/Palomar survey, galaxies brighter than $m_{R,AB} = 24.1$ are selected and split by star formation rate: star-forming ($> 0.2 M_{\odot}/\text{yr}$; blue) and quiescent ($< 0.2 M_{\odot}/\text{yr}$; red). The large black circle indicates the location of the observer. The lightcone is split into sections to fit on the page. Starting from the observer, the lightcones runs from left to right (with distance and redshift increasing along the lightcone). At the right hand edge of the page the lightcone reappears on the left hand side, shifted up the page by $60 \text{Mpc}/h$. Significant large scale structures—some of which span the width of the lightcone—are apparent, highlighting the need for a careful analysis of sample variance.

We begin by populating the entire Millennium Simulation with galaxies using the methods described in §3.2. This process is carried out for every available redshift in the Millennium Simulation between $z = 2$ and $z = 0$. In addition to physical properties such as stellar mass and star formation rate we compute for each galaxy observable quantities such as apparent magnitudes in several bands and rest-frame absolute magnitudes.

We then extract lightcones from this multi-redshift dataset using techniques similar to those of Kitzbichler & White (2007). The only significant difference lies in the method of interpolating galaxy properties between the output redshifts of the Millennium Simulation as discussed below. Briefly, we select random locations within the simulation volume and place an “observer” at that point. A line of sight is chosen following the methods of Kitzbichler & White

lightcone of an observer located at some point within the simulation volume.

(2007)⁶ and a cone with the geometry of the observed sample is constructed around this line of sight. We then proceed to identify all galaxies which intersect the past lightcone of the observer within this cone.

Kitzbichler & White compute magnitudes of each galaxy at its output redshift and the two adjacent output redshifts, thereby allowing them to interpolate to find the magnitude at any intermediate redshift. They effectively apply a differential k -correction to correct for the difference between the output redshift and the observed redshift at which the galaxy intersects the past lightcone. In our approach, we track each galaxy from one output to the next.

⁶ The lightcones constructed have an extent much greater than the size of the Millennium Simulation and so use the periodic boundary conditions of the simulation to effectively create a larger volume. The methods of Kitzbichler & White (2007) choose the line of sight in such a way as to minimize the possibility of the cone intersecting the same region of the simulation in different periodic replications.

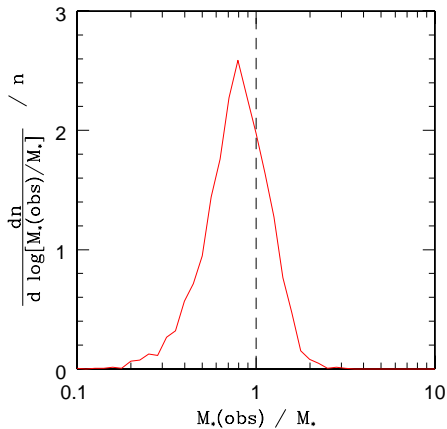


Figure 5. The stellar masses of a representative 15,000 galaxies, derived from the simulated photometry, plotted as a fraction of the generated stellar mass. The IMF of Chabrier (2003) was used in the model and in the analysis used to make the mass estimates.

Consequently, we can directly interpolate the properties of the galaxy to the precise redshift at which it is observed. Importantly, this allows us to include both k -corrections and evolutionary corrections to magnitudes and to interpolate stellar masses which will change from one output to the next.

Twenty lightcones are constructed, each having a solid angle of 0.42deg^2 , equivalent to the largest individual area covered by any of the three DEEP2/Palomar sub-samples. Galaxies are selected from within each lightcone if their R_{AB} and K_s magnitudes fall within the same limits as the observational sample. The variation in number density across these 20 samples can then be calculated.

We create additional sets of lightcones by trimming the originals to match the solid angles of the smaller DEEP2/Palomar fields which are relevant at $0.7 < z < 1.0$ (see Table 2). For these redshifts, 4845 mock samples are generated, each consisting of four lightcones of the appropriate size, and the variation measured across these samples. The estimates of sample variance obtained in this way are therefore conservative; slight underestimates because of correlations between the different lightcones.

3.4 Stellar mass estimates

Stellar masses in the DEEP2/Palomar survey were derived for each survey galaxy using the spectroscopic redshift (when available) and a spectral energy distribution (SED) based on optical and near-infrared photometry. The effect of possible errors in this process were discussed in detail by Bundy et al. (2006). In the case of the simulated galaxies, we can evaluate the uncertainties independently by computing predicted photometric magnitudes using GALFORM and then applying the same method used by Bundy et al. (2006) on the observed photometry to rederive stellar mass estimates. Comparing these derived masses to the “input” values determined by the model provides a useful check on the stellar mass estimates and their uncertainties.

For each of 15,000 galaxies, the predicted photometry for model galaxies was compared to actual data from the EGS field of the DEEP2 survey. Photometric errors were as-

signed by randomly sampling the error distribution of EGS sources with similar magnitudes for each passband. In this way the perturbed magnitudes of the simulated galaxies reflect the data quality of the EGS, including the variations in survey depth. The stellar mass was estimated as in Bundy et al. (2006) by comparing the “observable” SED of model galaxies to a large grid of stellar population templates and marginalizing over this grid, the final value being the median of the mass probability distribution.

The comparison between the derived mass estimates and their input values are shown in Figure 5. For most galaxies, the agreement is excellent with a scatter of ~ 0.15 dex as expected from the analysis in Bundy et al. (2006) of the internal uncertainties of the mass estimator and photometric errors. This level of uncertainty is applied to the model masses when constructing mass functions below. Our mass comparison also identified a small subclass of model galaxies where the rederived mass estimates are larger by ~ 0.1 dex than their model values. These systems are of intermediate mass and have star formation histories that have been sharply truncated by the GALFORM model, usually as a result of entering a larger halo. The timescales are typically much shorter than a dynamical time, leading to unphysical stellar populations that are poorly fit by the stellar mass estimator. Indeed, these galaxies populate a region of colour-colour space that is avoided by observed galaxies and represent the extreme end of the problem of over-quenching, which we will return to below.

4 RESULTS

Our primary goal is to compare the downsizing trends claimed by Bundy et al. (2006) via their colour-dependent stellar mass functions and to address the extent to which their evolving mass threshold is consistent with feedback models which reproduce the local mass and luminosity function (Bower et al. 2006; Croton et al. 2006).

4.1 Colour bimodality and the quenching of star formation

We begin our comparison between the DEEP2/Palomar observations and the GALFORM model with an analysis of the colour distribution. Figure 6 plots in three redshift intervals the restframe ($U - B$) colour-magnitude diagram of galaxies drawn from one set of mock lightcones constructed to match the properties of the DEEP2/Palomar dataset. As discussed in Croton et al. (2006) and Bower et al. (2006), Figure 6 shows that the incorporation of radio-mode AGN feedback helps establish a distinct red sequence and prevents star formation in the brightest galaxies, as observed. The solid line in these diagrams has a slope given by van Dokkum et al. (2006) with a vertical offset chosen empirically by Willmer et al. (2006) and Bundy et al. (2006) to divide the red sequence from the blue cloud in the observed DEEP2 distribution. This line has the equation:

$$U_r - B_r = -0.032(B_r + 21.5) + 0.454 - 0.25 \quad (7)$$

Clearly the colour cut defined by the observational data appears sub-optimal to split the model sample. A more appropriate cut (solid line) is therefore used in the investiga-

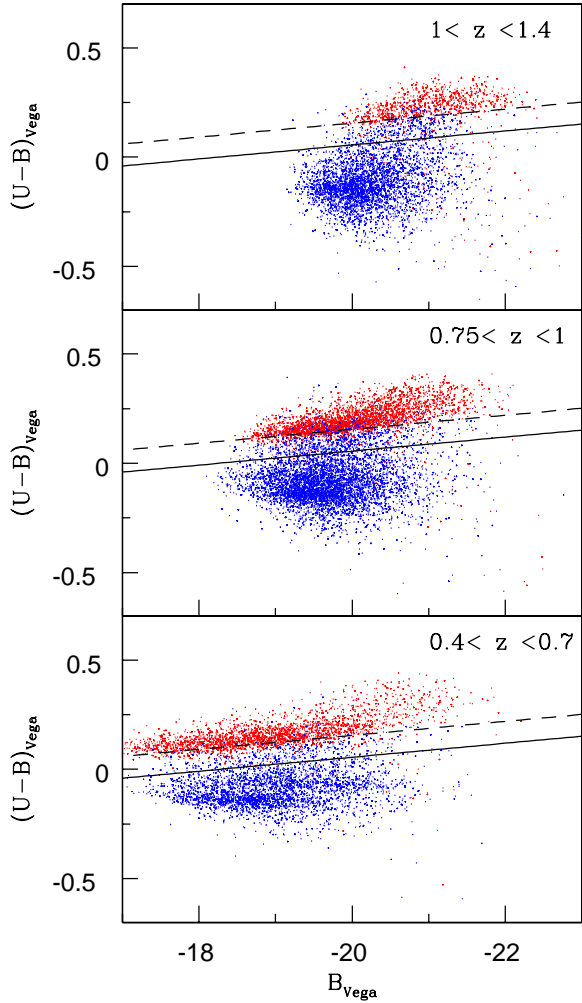


Figure 6. Galaxies from one of the 20 lightcone samples. As in Bundy et al. (2006), the star-forming and red-sequence galaxies are highlighted by applying a cut on the star formation rate at $\dot{M}_* = 0.2M_\odot\text{Gyr}^{-1}$. Galaxies above this cut are coloured blue while those below are coloured red in Figure 6. This criterion serves to illustrate the presence of two distinct populations but it does not identify each precisely. The solid diagonal line indicates the division made in the *observational* sample using rest-frame $U - B$ colours. The solid line shows the division in the *model* sample, thereby producing Figures 8 & 9.

tion into the evolution of these two populations (§4.2 and 4.3). We note that this adjustment did not significantly change the relative fraction of red and blue galaxies, since the bulk of the red population remain above the dotted, observational line in Figure 6.

A more profound discrepancy between the observed and modelled colours is shown in Figure 7 which plots the $(U - B)$ distribution in the same three redshift intervals. Results from the lightcones are illustrated by shaded curves while data points signify the observed distributions from the DEEP2/Palomar dataset. Beginning with the total distribution, we find that model galaxies trace a narrower range in $(U - B)$ colour than observed galaxies. Even after including photometric uncertainties of 0.1 mag, the distribution of colours is simply too narrow, particularly at low redshift.

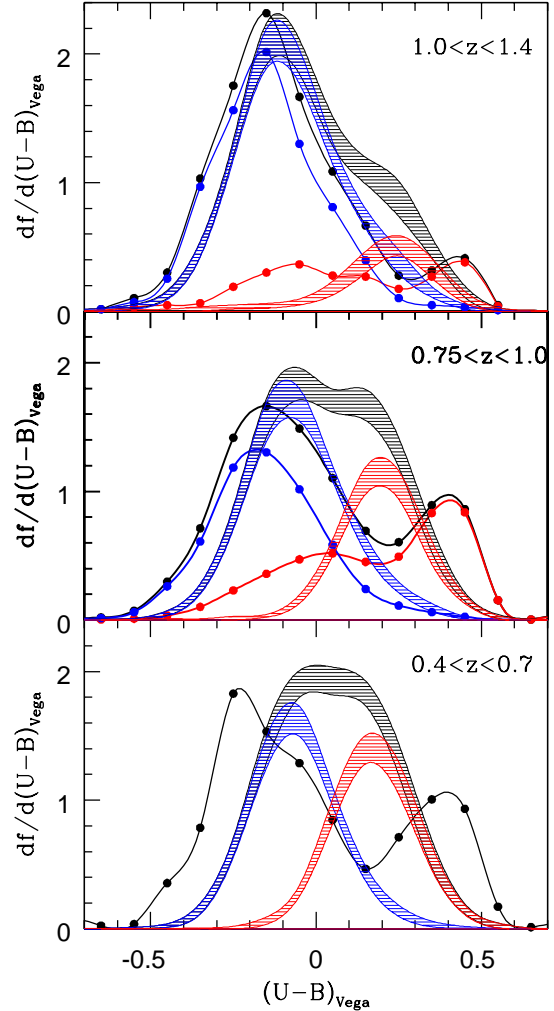


Figure 7. The rest-frame $U - B$ colour distribution. Black points show observational values and shaded areas correspond to the total range of values found across 20 lightcones. For the latter, an observational error of 0.1 mag (1 s.d.) has been included. Both datasets are connected with smooth curves for visual clarity. The same star formation rate cut as Figure 6, $\dot{M}_* = 0.2M_\odot\text{Gyr}^{-1}$, is applied to illustrate the division into two populations.

Figure 7 reveals further insight into the problem that the GALFORM model has in reproducing the red sequence. The total distribution shows evidence for a red sequence in the two highest redshift bins, while for $0.4 < z < 0.7$ the colour distribution looks nearly unimodal. Even in the two high- z bins the red-sequence is offset blueward of the data—as we saw in Figure 6—and seems to include larger numbers of red systems than observed.

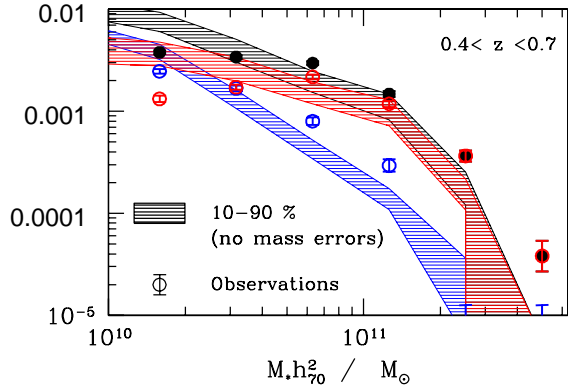


Figure 8. The effect of cosmic variance on the derived stellar mass function at $0.4 < z < 0.7$. Points are observational values from Bundy et al. (2006). Shaded areas show the 10-90% range of the simulated mass functions generated from 20 lightcones, defined as discussed in section 3.3. Black points and shading relate to the total mass function; red and blue to quiescent and star-forming components, divided as shown in Figure 6. Note that, in this figure, stellar masses are taken directly from the model, with no inclusion of errors arising from photometric uncertainties. The effect of including errors can be seen by comparison with the bottom panel of Figure 9.

4.2 Evolution of the total mass function

Despite the disagreement between the predicted and observed restframe colour distributions, we can still evaluate whether the current feedback prescriptions reproduce the general mass-dependent decline of star formation in galaxies since $z \sim 1$ which represents the basic ‘downsizing’ signature. Such a signature should not be too dependent on the precise definition of what constitutes a quiescent or active galaxy.

We begin by comparing the total mass function from both the mock lightcones and the observations. The results from the model are plotted in Figure 9 as the black shaded regions while the observations are indicated by black solid points. The width of the shading shows the 10-90% range of values recovered from the lightcone samples. As emphasized by Kitzbichler & White (2007), we find good agreement with the observed total mass function *when the stellar mass uncertainties are convolved with the model results*. This has the effect of increasing the high-mass end of the predicted mass function, as can be seen by comparing Figures 8 and 9. We note that we observe fewer low-mass galaxies than predicted at all redshifts, despite the extremely efficient conversion of supernova energy to ejected gas in this model (§3.2). The completeness issues in the observational sample do not explain this discrepancy because the observational magnitude limits have been included in the mock lightcones.

Though disagreement between the predicted and observed total numbers appears to be minor, this thorough analysis of cosmic variance shows that there is still *significant inconsistency* with the data at many stellar mass intervals.

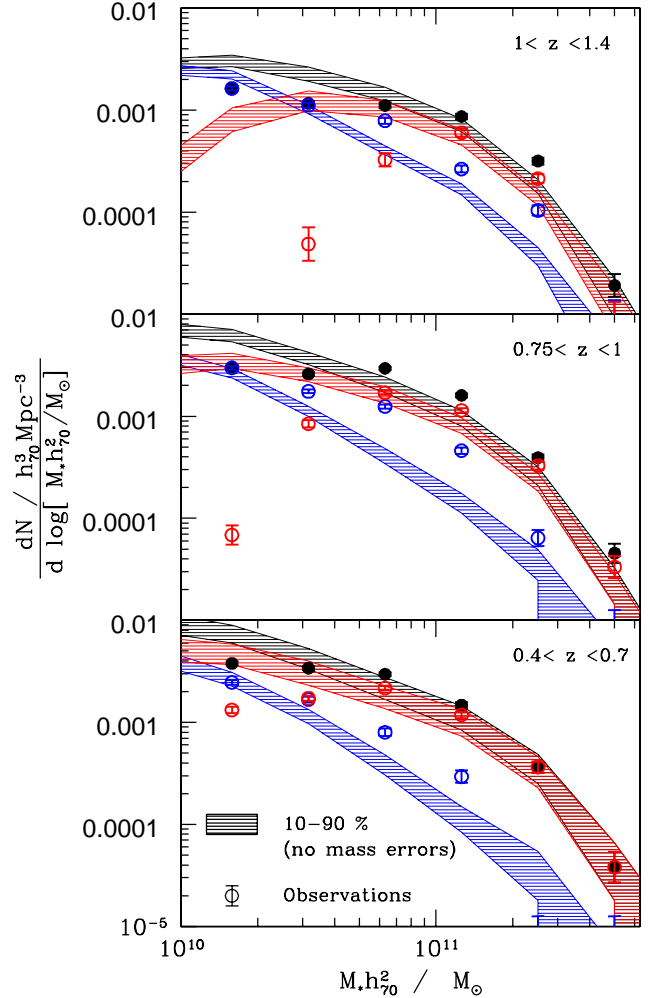


Figure 9. The evolving stellar mass function from the DEEP2/Palomar survey compared with the output of the semi-analytic models using the GALFORM radio-mode feedback. The predictions include the effect of errors in the stellar mass determination. The 10-90% range of the various lightcone realizations are indicated by the shaded areas. All lightcones are reduced in size so that the four solid angles in each set correspond to those of the four DEEP2/Palomar survey fields (see Table 2). The significance of the colours is consistent with Figure 8. According to Bundy et al. (2006), the mass completeness limits from the K_S -band alone are $\log[M_*/M_\odot] = 10.1, 10.2$ and 10.4 for the three respective redshift intervals.

4.3 Verifying a decline in the star-forming population

By adopting a suitable division in colour (Fig. 6), the model galaxies are divided into red sequence and star-forming populations. It is clear from Figure 9 that the resulting component mass functions fail significantly to match the observed numbers, even after allowing for cosmic variance and mass errors. However, one important evolutionary trend is qualitatively similar; the red-sequence population growing with time. The blue population in the model shows no significant evolution however, remaining static across the entire redshift range while the observed numbers fall with time. This leads

us to address an important discrepancy of interpretation in the *observed* mass functions.

Bundy et al. (2006) argue that massive blue galaxies detected at $z \sim 1$ increasingly transform into quenched red systems, leaving the total mass function relatively unchanged since $z \sim 1$. Faber et al. (2007) analyze B -band luminosity functions from DEEP2 and COMBO17 and argue that the number of blue galaxies is essentially unchanging, with the increase in the massive red sequence population coming primarily from ‘dry mergers’ - mergers of similarly quiescent galaxies. Bell et al. (2007) invoke a third option in which the red sequence is built primarily from quenched blue galaxies that are quickly replenished, leaving their numbers unchanged. The uncertain effects of cosmic variance have made distinguishing these scenarios challenging. With the improved measure of sample variance afforded by our multiple lightcones, we can now evaluate the validity of these claims.

The fundamental question is whether the evolution in the mass function of blue, star-forming galaxies claimed by Bundy et al. (2006) is significant given the uncertainties of cosmic variance. We have re-analyzed the observational results of Bundy et al. (2006) to derive upper limits on the blue mass function at the high mass end for the two lower redshift intervals. These upper limits are determined by the value that would have been obtained had one blue galaxy been detected in each bin. In all cases, the upper limits are $dn/d \log(M_*/M_\odot) < 10^{-4.9} \text{Mpc}^{-3}$.

As is apparent in Figure 9, this analysis reinforces the substantial decline observed in blue galaxies—nearly an order of magnitude across the redshift range at $\log(M_*/M_\odot) \approx 11.4$. This decrease is significant at the 99.9% level. The other mass bins above the R -band determined completeness limit of $\log(M_*/M_\odot) \approx 10.9$ do not show significant evolution, however. Using the upper limits, we find no evolution in the highest mass bin, $\log(M_*/M_\odot) = 11.7$. It should be noted that no blue galaxies were detected at these masses with $z < 1.0$, so this result is a lower limit on potential evolution. At $\log(M_*/M_\odot) = 11.1$, the observations show an increase from $z \approx 1.2$ to $z \approx 0.9$ followed by an equally significant decrease from $z \approx 0.9$ to $z \approx 0.5$. Across the full redshift range, this is consistent with no evolution in the $\log(M_*/M_\odot) = 11.1$ mass bin at the 60% level.

Taken together, Figure 9 and the analysis above substantiates the claim made by Bundy et al. (2006) that the population blue, star-forming galaxies observed at $z \sim 1$ declines with time beyond the quenching mass, $\log(M_*/M_\odot) > 11.2$ (Bundy et al. 2006). We note, however, that this evolution is not easy to detect even in the large DEEP2/Palomar dataset. Although we see strong and significant evolution in one mass bin, averaging over the relevant mass range reduces the significance to the $2\text{--}3\sigma$ level after cosmic variance.

Still, such evolution suggests that the red sequence is primarily built from the quenching of star-forming galaxies and only to a lesser extent from dry merging. A replenishing supply of blue systems would not seem to be necessary since such galaxies are not detected at lower redshifts. Finally, the substantial uncertainties from cosmic variance, which dominate the error budget, mean that much larger data sets will be required for more detailed studies capable of quantifying the importance of such effects as merging, internal growth due to SF, and transformations on the mass functions of

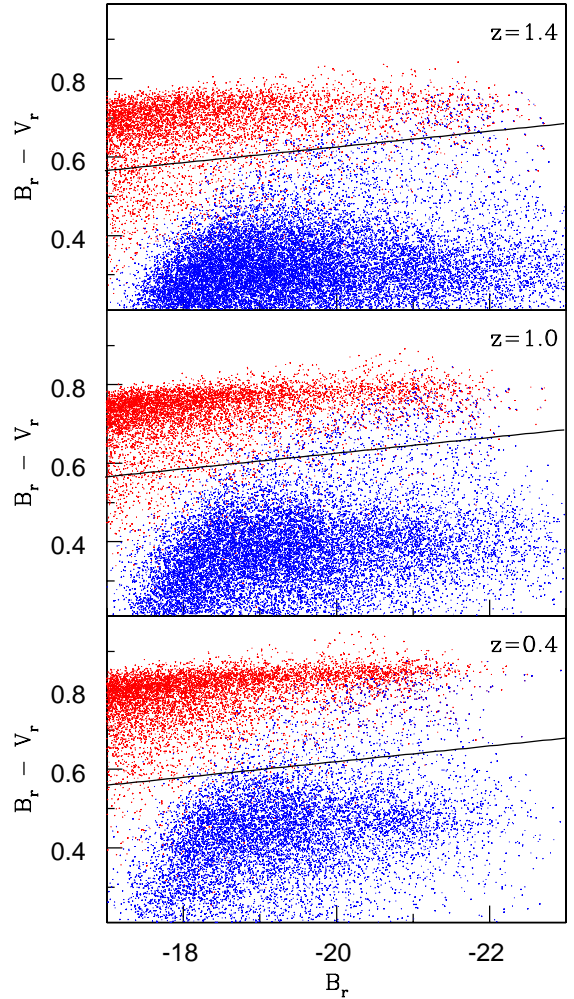


Figure 11. The colour magnitude distribution of all the galaxies in a subvolume of the simulation, generated using the model of De Lucia & Blaizot (2007). The solid black line indicates the colour divide applied to create Fig. 10.

different types of galaxies. Such work will represent an important step forward in understanding the physical nature of the quenching mechanism. In Section 4.5, these limitations are discussed in the context of upcoming surveys.

4.4 Alternative models

The method applied by Bower et al. (2006), populating the halos of the Millennium simulation using a galaxy formation model, was also adopted by Croton et al. (2006). The results from an updated version of this model (De Lucia & Blaizot 2007) have been made publically available⁷ and the stellar masses and colours of all the galaxies in the simulation volume were extracted.

There are some significant differences in the way that some of the physical processes are modelled. Star formation is assumed to occur only if there is sufficient gas to exceed a critical surface density, following the work of Martin &

⁷ <http://www.g-vo.org/Millennium>

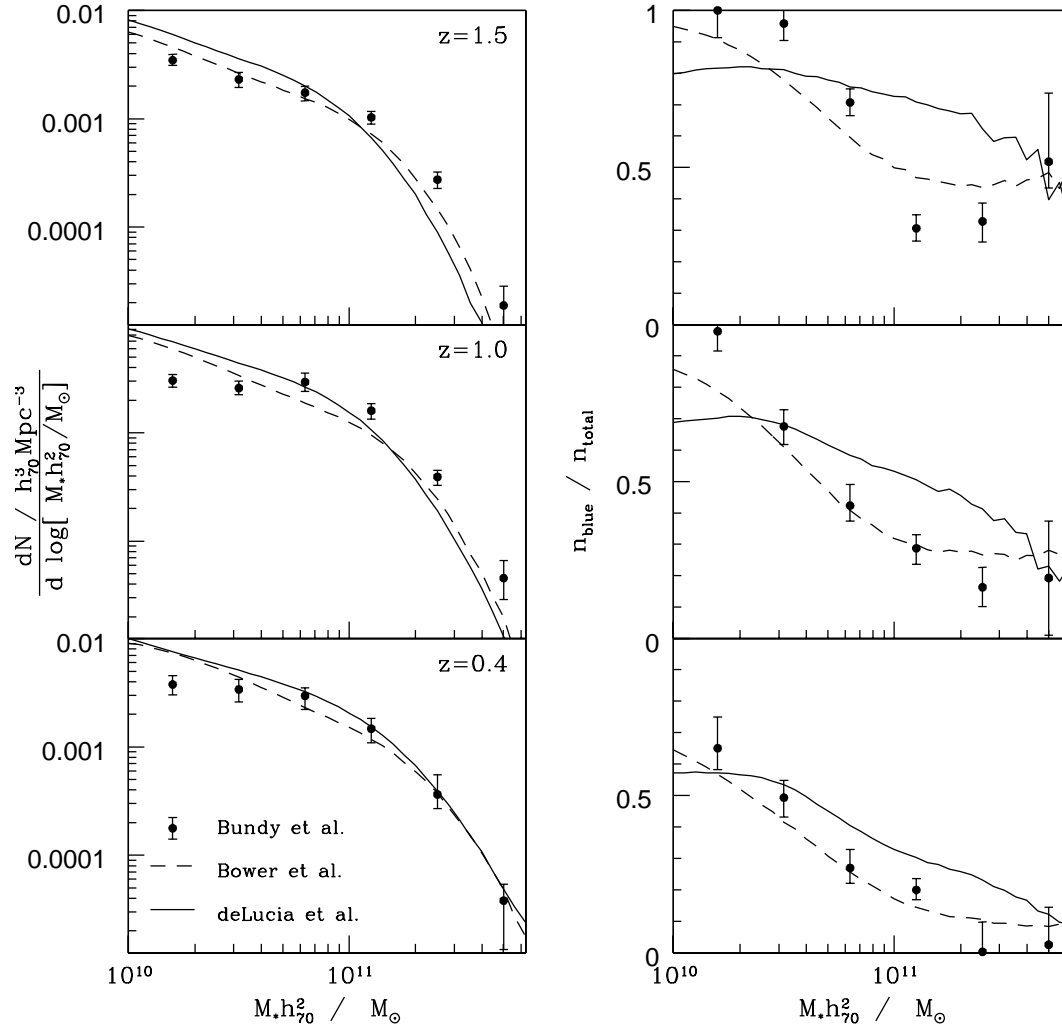


Figure 10. Comparison between the stellar mass function predicted by the modelling technique and parameters of Bower et al. (2006) (dotted lines) and those of De Lucia & Blaizot (2007) (solid lines). Both build on the halo population of the Millennium simulation. They are divided into two populations using the dividing criteria illustrated in Figures 6 and 11. Points show the observational determinations of Bundy et al. (2006), but now with error-bars that reflect the cosmic variance calculated using the techniques of section 3.3. The points are from samples limited in magnitude at $R=24.1$ (except the highest redshift, which shows the photo- z supplemented mass function from Bundy et al. (2006), limited at $R=25.1$). Since the model mass functions are derived from instantaneous snapshots from the simulation (not from lightcones) the data is therefore included for reference, not for strict comparison.

Kennicutt (2001). The mass converted into stars is then 5–15% of the gas which is above this value. This approach can be compared with equation (2). Gas is reheated from the disk in line with equation (3) but with $\beta = 3.5$; the halo potential is involved only when calculating the gas ejected from the halo, not from the disk.

AGN feedback is also incorporated, but rather than imposing a cut-off black hole mass which prevents cooling completely, the cooling rate is simply modified:

$$M'_{\text{cool}} = M_{\text{cool}} - \frac{\eta \dot{M}_{\text{BH}} c^2}{\frac{1}{2} v_{\text{vir}}^2}. \quad (8)$$

The efficiency, $\eta = 0.1$. Black hole accretion in this model is also set to match the $M_{\text{BH}} - M_{\text{bulge}}$ relation mentioned in section 3.2.

The stellar mass function derived from both models is shown in the left hand panel of Figure 10, for the same red-

shift ranges as before. It is worth emphasising that these number densities are not derived from lightcone samples, but from the entire volume. The points from the observational sample are therefore included in Figure 10 for *qualitative comparison only*. Detailed quantitative analysis was possible using Figure 9, which sets the data against correctly constructed mock observations.

Despite some considerable differences in their physical assumptions and choice of parameters, it is clear that both models produce very similar predictions. This similarity reflects the fact that those parameters which remain theoretically uncertain are chosen to match each of the models to certain observational data. Similar data sets will have been used in both cases, and will have included the stellar mass function at $z = 0$. This partly accounts for the fact that the two models agree more closely with each other (and with the observations) at lower redshift.

In both cases, the predicted stellar mass function evolves in qualitative agreement with these observations. Major disagreement is restricted to distant, low mass galaxies where survey completeness may provide an immediate explanation.

The colour distribution of galaxies in this second model also shows a clear bimodality (Fig. 11), as discussed in Croton et al. (2006). The distribution is reproduced here to show the division between red and blue populations which has been used to produce the right hand panel of Figure 10, showing their fractional abundance. As with the total number density, both models correctly predict the trend for the blue fraction to decrease with mass and increase with redshift, but specific values are frequently inconsistent with observations.

The data points in Figure 10 have updated error-bars which now reflect the cosmic variance estimates shown in Figure 9. The *difference* between the two models is rarely more than this cosmic variance, illustrating an inherent difficulty in constraining competing theories of galaxy evolution on the basis of their predicted stellar mass functions.

4.5 The effect of cosmic variance on present & future surveys

A salutary lesson from Figure 9 is that even with the largest and most complete survey of the evolving stellar mass function to date, cosmic variance is still limiting quantitative conclusions concerning the growth rate of massive galaxies ($M_* > 10^{11} M_\odot$) at the level of factors of order 2-3. These uncertainties have a larger impact than errors in the stellar mass (§3.4).

Given we have developed the machinery to address this uncertainty, it is interesting to know the extent to which present and upcoming surveys will be limited by cosmic variance in addressing basic questions: what is the assembly rate of the most massive galaxies from $z < 2$ to the present day?

In an important paper, Somerville et al. (2004) introduced a simple analytical approach for estimating the effects of cosmic variance in a survey. These analytical estimates can be calculated for our mock samples by following the definition used in Somerville et al. (2004):

$$\sigma_V^2 \equiv \frac{\langle N^2 \rangle - \langle N \rangle^2}{\langle N \rangle^2} - \frac{1}{\langle N \rangle}. \quad (9)$$

It can also be calculated using the correlation length, which is available for the DEEP2 survey (Coil et al. 2008). Figure 12 compares this analytical prediction with the variance derived directly from our multiple lightcones technique. As can be seen, the relative agreement is quite encouraging.

Returning to the physical questions posed above. Figure 13 shows the number density of intermediate-mass ($10^{10} < M/M_\odot < 10^{11}$) and high-mass ($M > 10^{11} M_\odot$) galaxies for the entire volume of the Millennium Simulation. The key question is the extent to which present and upcoming surveys can verify not only the basic trends of mass assembly but also the mass-dependent variations.

First, we consider the situation for the data evaluated in the present paper. For the Bundy et al. (2006) data plotted in Figure 13, errors correspond to the 10-90% range of values found from the 20 lightcone realizations of this survey. Over $0 < z < 1.4$, the predicted growth trends in intermediate mass

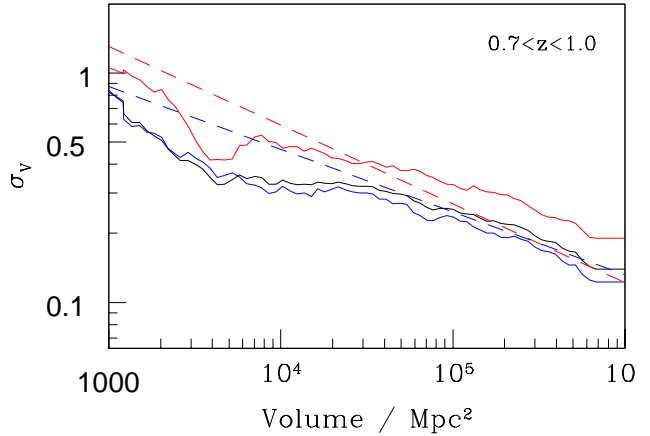


Figure 12. The relative cosmic variance of the red and blue galaxy populations as a function of survey volume. The solid lines are calculated using the 20 lightcones, the dotted lines using the analytical approach of Somerville et al. (2004) (see text). The relative variance of the total population of galaxies across the 20 lightcones is shown in black.

Table 2. Some details of the selection of observational surveys referenced in Figure 13.

Field	Area/deg ²	Mag. Limits	
		R_{AB}	K_{vega}
EGS & DEEP2	Table 1	24.1	20.5
GOODS North	1×0.042	24.1	21
COSMOS	1×1.5	25	22
UKIDSS	$\left\{ \begin{array}{l} \text{D.E.S.} \\ \text{U.D.S.} \end{array} \right.$	4×8.75	23
		1×0.77	27

galaxies (upper, black line) are only marginally confirmed and the predicted growth in massive galaxies (lower, red line) is inconsistent with observations.

Much of the differential trends observed are affected by the area of the survey and the optical magnitude limit (Table 2). The situation with earlier HST samples (GOODS, Giavalisco et al. (2004)) is considerably worse. However, even with upcoming panoramic surveys underway with HST (COSMOS, Scoville et al. (2007)) and UKIRT (UKIDSS, Lawrence et al. (2007)), the situation is not significantly better. Thus precise observational constraints concerning the *differential evolution* of mass assembly must await a future generation of surveys.

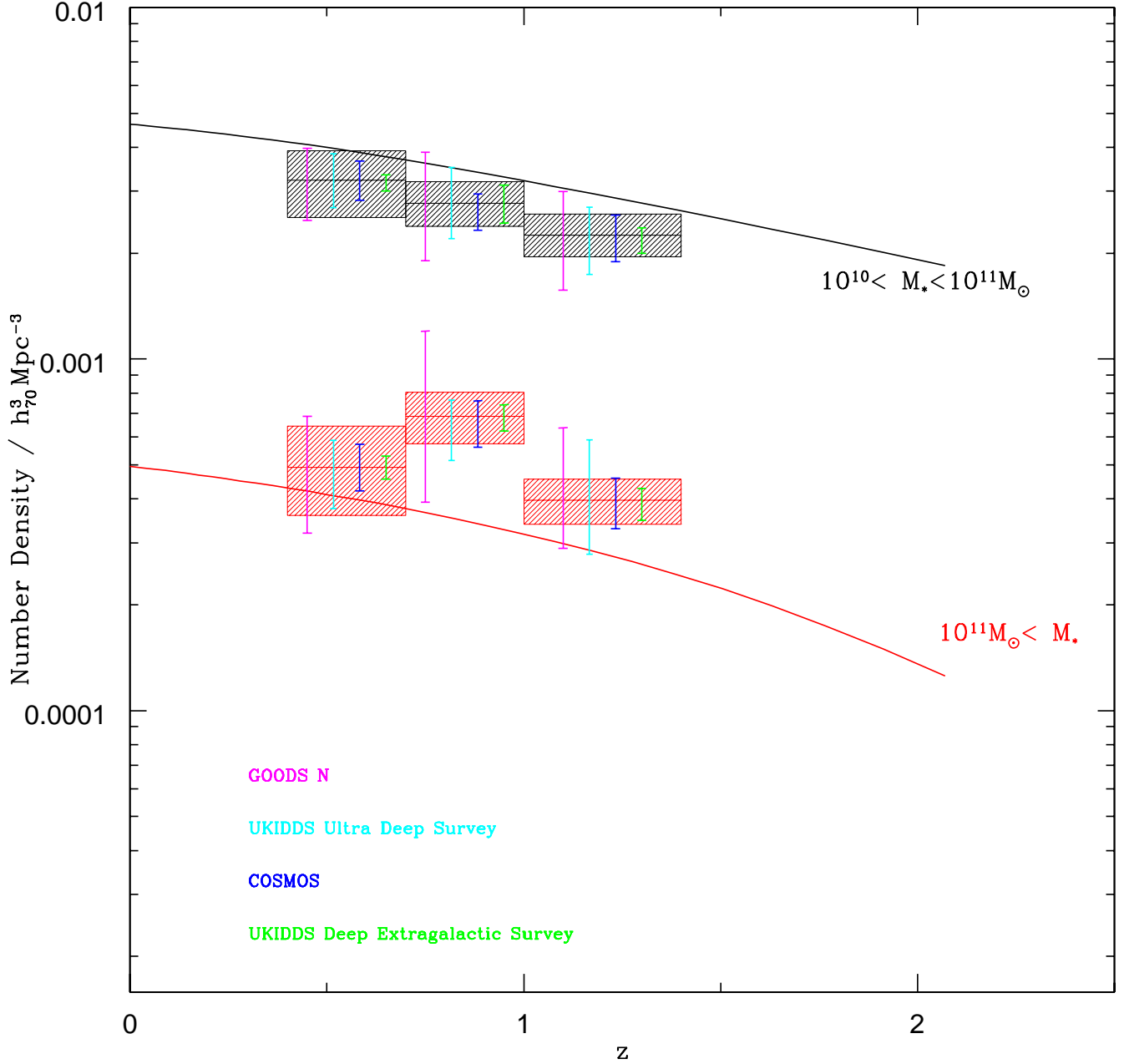


Figure 13. The predicted comoving number density of galaxies derived from the full volume of the Millennium Simulation for intermediate-mass galaxies (black curves) and those with high stellar mass (red curves). Shaded areas indicate the constraints on mass assembly in these two mass bins according to the results of Bundy et al. (2006). The mean number densities for $10 < \log(M_*/M_\odot) < 11$ may be affected by some incompleteness, which becomes important at $\log(M_*/M_\odot) < 10.4$ in the photo-z supplemented sample used here ($R_{AB} < 25.1$). However, the mock observations confirm that most of the discrepancy between the data and the models at lower masses is real and not simply the result of incompleteness (Fig.9). The shading indicates 10-90 % error due to cosmic variance, calculated using the techniques described in §3.3. Error bars illustrate the equivalent error expected in other present and upcoming surveys (left to right are listed from top to bottom). For convenient comparison, these errors are all given relative to the same, observationally determined mean densities.

5 SUMMARY

Lightcones derived from the Millenium Simulation, designed specifically to match the geometry and selection parameters of the DEEP2/Palomar survey of Bundy et al (2006), reproduce reasonably well the evolving stellar mass function over $0.4 < z < 1.2$. These mock observations are populated with galaxies using the GALFORM code, which incorporates a prescription for ‘radio mode’ feedback. Such feedback processes are thus an adequate explanation of the broad trend of ‘downsizing’ seen in recent redshift surveys.

However, the GALFORM code can not satisfactorily reproduce the evolving form of the bimodal colour distribution, or the stellar mass functions of the corresponding two populations. An alternative model (De Lucia & Blaizot 2007), proposed originally by Croton et al. (2006), produces similar discrepancies; both models appear to over-quench star formation in intermediate mass galaxies.

This approach also allows us to address the important question of how cosmic variance may limit the validity of various conclusions drawn from observational surveys. Using variance estimates derived from the lightcones, we confirm the significance of the decline since $z \simeq 1$ in the number density of massive blue galaxies claimed by Bundy et al (2006). We argue that the transformation of these blue galaxies must, necessarily, provide the bulk of the associated growth in red sequence galaxies given the near-constant total mass function.

This discussion of cosmic variance is extended to demonstrate the limitations of other, more ambitious, surveys ongoing at the present time in terms of detecting the *mass-dependent* growth of galaxies since $z \simeq 1$.

ACKNOWLEDGMENTS

We would like to thank Carlton Baugh, Richard Bower, Shaun Cole, Carlos Frenk, John Helly, Cedric Lacey and Rowena Malbon for allowing us to use the GALFORM semi-analytic model of galaxy formation (www.galform.org) in this work. We also thank Simon White for helpful comments.

The Millennium Run simulation used in this paper was carried out by the Virgo Supercomputing Consortium at the Computing Centre of the Max-Planck Society in Garching. The databases and the web application providing online access to them were constructed as part of the activities of the German Astrophysical Virtual Observatory <http://www.g-vo.org/Millennium>.

MJS acknowledges support from the Warden and Fellows of New College, Oxford, the hospitality of the CTCP at Caltech and of the KITP, Santa Barbara. AJB acknowledges support from the Gordon & Betty Moore Foundation. RSE acknowledges financial support from the Royal Society.

REFERENCES

Baugh, C. M., Lacey, C. G., Frenk, C. S., Granato, G. L., Silva, L., Bressan, A., Benson, A. J., & Cole, S. 2005, MNRAS, 356, 1191
 Bell E. F., Zheng X. Z., Papovich C., Borch A., Wolf C. & Meisenheimer K., 2007, ApJ, 663, 834

Benson, A. J., Bower, R. G., Frenk, C. S., Lacey, C. G., Baugh, C. M., Cole, S. 2003, ApJ, 599, 38
 Birnboim, Y., Dekel, A., 2003, MNRAS, 345, 349
 Borch, A., et al. 2006, A&A, 453, 869
 Bower, R. G., Benson, A. J., Malbon, R., Helly, J. C., Frenk, C. S., Baugh, C. M., Cole, S. & Lacey, C. G. 2006, MNRAS, 370, 645
 Bundy, K., Ellis, R. S., & Conselice, C. J. 2005, ApJ, 625, 621
 Bundy, K., et al. 2006, ApJ, 651, 120
 Brinchmann J. & Ellis R.S., 2000, ApJ, 536, 77
 Cattaneo, A., Dekel, A., Faber, S. M., Guideroni, B. 2008, arXiv:0801.1673
 Chabrier, G. 2003, PASP, 115, 763
 Cimatti, A., et al. 2004, Nature, 430, 184
 Coil, A. L. et al. 2008, ApJ, 672, 153
 Cole S., Lacey C., Baugh C. & Frenk C. 2000, MNRAS, 319, 168
 Cole S. et al. 2001, MNRAS, 326, 255
 Croton, D. J., et al. 2006, MNRAS, 365, 11
 Davis, M. et al. 2003, Proc. SPIE, 4834, 161
 De Lucia, G., & Blaizot, J. 2007, MNRAS, 375, 2
 Drory N., Bender R. & Hopp U., 2004, ApJ, 616, 103
 Efsthathiou G., Lake G., Negroponte J. 1982, MNRAS, 199, 1069
 Eke, V. R., Cole, S., Frenk, C. S. & Henry, J. P. 1998, MNRAS, 298, 1145
 Faber S. M. et al. 2007, ApJ, 665, 265
 Fontana A. et al., 2004, AA, 424,23
 Giavalisco, M. et al., 2004, ApJ, 600, L93
 Glazebrook, K. et al. 2004, Nature, 430, 181
 Guzman, R, et al. 1997, ApJ, 489, 559
 Harker G., Cole S., Helly J., Frenk C. S., Jenkins A., 2006, MNRAS, 367, 1039
 Häring, N., & Rix, H.-W. 2004, ApJ, 604, L89
 Helly J. C., Cole S., Frenk C. S., Baugh C. M., Benson A. J., Lacey C., 2003, MNRAS, 338, 903
 Hopkins, P. F., Bundy, K., Hernquist, L., & Ellis, R. S. 2007, ApJ, 659, 976
 Kauffmann G., Colberg J. M., Diaferio, A. & White, S. D. M. 1999, MNRAS, 303, 188
 Kauffmann G. et al., 2003, MNRAS, 341, 54
 Kennicutt, R. C., Jr. 1983, ApJ, 272, 54
 Kennicutt R. C., 1998, Annual Review of Astronomy & Astrophysics, 36, 189
 Keres D., Katz N., Weinberg D. H., Davé R., 2005, MNRAS, 363, 2
 Kitzbichler M. G. & White S. D. M., 2006, MNRAS, 366, 858
 Kitzbichler M. G., & White, S. D. M. 2007, MNRAS, 376, 2
 Lawrence A., et al. 2007, MNRAS, 379, 1599
 Le Fèvre, O. et al., 2005, 439, 845
 Martin, C. L., & Kennicutt, R. C., Jr. 2001, ApJ, 555, 301
 McCarthy I. G., Frenk C. S., Font A. S., Lacey C. G., Bower R. G., Mitchell N. L., Balogh M. L., Theuns T., 2008, MNRAS, 383, 593
 McKee C. F. & Ostriker J. P., 1977, ApJ, 218, 148
 Navarro J. F., Frenk C. S. & White S. D. M., 1995, MNRAS, 275, 720
 Pozzetti L, et al. 2007, AA, 474, 443
 Scoville, N., et al. 2007, ApJS, 172, 38
 Somerville R. S. & Primack J. R. 1999, MNRAS, 310, 1087
 Somerville R. S., Lee K., Ferguson H. C., Gardner J. P., Moustakas L A., & Giavalisco M. 2004, ApJ, 600, L171
 Springel, V., White, S. D. M. & Jenkins, A., 2005, Nat, 435, 629
 Springel, V., Di Matteo, T., & Hernquist, L. 2005, MNRAS, 361, 776
 Sutherland R. S. & Dopita M. A., 1993, ApJ, 88, 253
 van Dokkum, P. G. et al. 2006, ApJ, 638, L59
 Willmer, C. N. A et al. 2006, ApJ, 647, 853
 Wolf C., Meisenheimer K., Rix H.-W., Borch A., Dye S. & Kleinheinrich M., 2003, AA, 401, 73

APPENDIX A: STAR FORMATION EFFICIENCY

In this Appendix we illustrate the importance of gas ejection from the disk, which was given in eqn. (3), for determining the stellar masses of galaxies. The differential equation which controls the mass of cold disk gas, M_{cold} , is

$$\dot{M}_{\text{cold}} = \dot{M}_{\text{in}} - (1 - R + \beta) \frac{M_{\text{cold}}}{\tau_{\star}}. \quad (\text{A1})$$

where $\tau_{\star} = \tau_{\text{disk}}/\epsilon_{\star}/(v_{\text{disk}}/200\text{km/s})^{3/2}$. The parameter $R = 0.39$ is the fraction of material in stars which will be recycled back into the interstellar medium in the instantaneous recycling approximation⁸.

For the relevant range of circular velocities, $5 < \beta < 10,000$, so outflow will be fierce and the only way that a significant supply of cold gas can be retained in the disk is through constant replenishment from the cooling halo gas. This corresponds to the limit $\dot{M}_{\text{cold}} \rightarrow 0$ for which equation (A1) has the following solution:

$$M_{\text{cold}} \approx \dot{M}_{\text{in}} \tau_{\text{eff}}, \quad \left[\tau_{\text{eff}} = \frac{\tau_{\star}}{1 - R + \beta} \right]. \quad (\text{A2})$$

Given the large values of β , the effective timescale, τ_{eff} will be extremely short, leading quickly to a steady state where the rates of cooling and reheating gas are approximately constant and equal. In this case, cold gas mass and star formation rate are given by:

$$M_{\text{cold}} \approx \dot{M}_{\text{in}} \tau_{\text{eff}}, \quad \dot{M}_{\star} \approx \dot{M}_{\text{in}} \frac{1 - R}{1 - R + \beta}. \quad (\text{A3})$$

(Note that the star formation rate given here is the rate of increase of mass in long-lived stars, hence the inclusion of the factor $1 - R$.) Because of the tendency towards these limits, the star formation rate in any particular galaxy is approximately constant (assuming a constant \dot{M}_{in}), ignoring short term perturbations resulting from mergers and gravitational instabilities which contribute little over cosmological timescales. In this approximation, the stellar mass is given by the star formation rate integrated over the available time, $t(z)$.

The specific star formation rates for galaxies at redshift z should therefore be expected to be scattered about the value

$$\frac{\dot{M}_{\star}(z)}{M_{\star}(z)} \approx \frac{1}{t(z)}. \quad (\text{A4})$$

Figure A1 demonstrates that these analytic approximations are broadly consistent with the calculated values for $\sim 400,000$ galaxies in a sub-volume of the model.

The above argument implies that specific star formation rate is *independent* of the equations which explicitly govern it. The parameters for star formation efficiency, ϵ_{\star} in eqn. (2), and the strength of outflow, β in eqn. (3) will have only a secondary influence of the underlying trend described by eqn. (A4).

⁸ This particular value is calculated from the initial mass function of Kennicutt (1983):

$$\zeta(M) \propto \begin{cases} M^{-1.4} & (0.1 \leq M \leq 1M_{\odot}) \\ M^{-2.5} & (1.0 \leq M \leq 100M_{\odot}) \end{cases}.$$

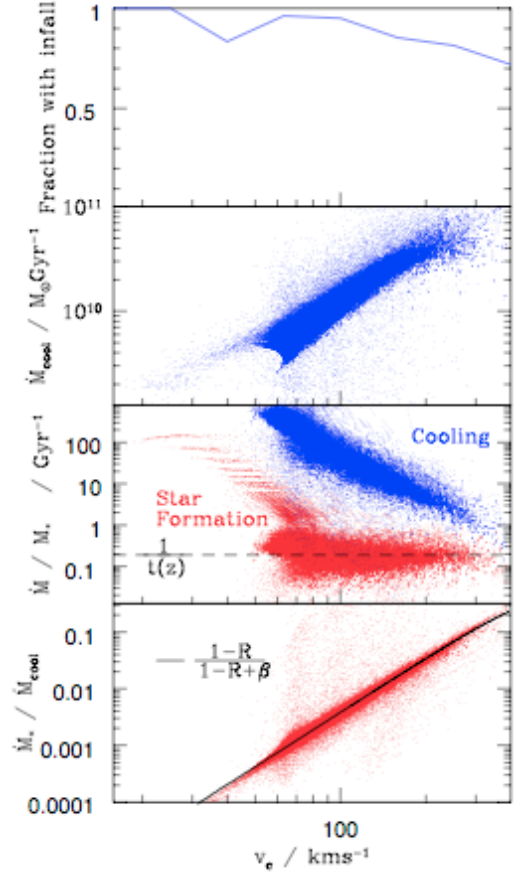


Figure A1. An illustration of the relationship between cooling rate and star formation rate as a function of disk circular speed, v_c for $\sim 400,000$ galaxies in an arbitrary sub-volume of the model at redshift $z = 0.5$. The top panel shows the (weighted) fraction of galaxies which have any cooling at all and so appear on the other three sets of axes. The second panel shows the cooling rate itself and the third panel shows both cooling rate and the star formation rate as a fraction of the existing stellar mass of each galaxy. The dashed line shows the constant star formation rate which would be required to accumulate the relevant stellar mass. The bottom panel illustrates that the ratio between the star formation and cooling is a function of the outflow efficiency, $\beta(v_c)$, as predicted by eqn. (A3).

The physical property which *is* controlled by the star formation efficiency is the mass of cold gas in the disk relative to the supply from the halo and, consequently, the stellar mass:

$$\frac{M_{\text{cold}}}{M_{\star}} \approx \frac{\tau_{\star}(\epsilon_{\star})}{t(z)}. \quad (\text{A5})$$

So, more efficient star formation leads to a lower gas fraction but *not* to higher star formation rates for galaxies of a given mass.

The cooling rate and outflow efficiency, β , determine the size of the halo in which a galaxy of a certain mass must reside in order to fuel its star formation. This is how the smaller-scale physics of star formation and supernovae influence the collective properties of galaxies on cosmological scales.